Relief threshold for eolian sand transport on alluvial fans

Joseph P. Cook[1] and Jon D. Pelletier[1]

Received 29 June 2006; revised 23 November 2006; accepted 15 February 2007; published 30 May 2007.

[1] Many arid alluvial-fan terraces downwind from eolian sand sources exhibit an abrupt increase in eolian epipedon thickness and sand content below a critical elevation which varies from fan to fan. Above this elevation, sand accumulates locally and is not transported across the fan. Below this elevation eolian sand from nearby playa and channel sources is readily transported across the distal fan. Here we test the hypothesis that these distal-fan eolian ''corridors'' are controlled by a threshold fan-surface relief. We propose that when along-strike relief falls below a critical threshold value, an eolian surface of transportation or ''corridor'' develops. To test this hypothesis, we measured multiple along-strike topographic profiles and eolian epipedon textures on two piedmonts in the Ivanpah Valley and adjacent Hidden Valley in Clark County, Nevada. Both piedmonts are located near sand-dominated playas and exhibit clear evidence of eolian transport across their distal fan regions. The near-surface boundary layer flow above each topographic profile was quantified using the multispectral finite difference (MSFD) numerical model. This model predicts the surface shear stress above complex terrain for any wind condition assuming neutrally stable flow. The minimum shear stress calculated by MSFD for each profile during extreme wind conditions was compared to the shear-velocity threshold necessary to initiate saltation. Model results showed that in proximal fan areas, along-strike relief was large enough to prevent eolian transport of all but fine sand particles. In distal fan profiles within the eolian corridor, model results predict shear stresses everywhere above threshold for both fine and coarse sand.

Citation: Cook, J. P., and J. D. Pelletier (2007), Relief threshold for eolian sand transport on alluvial fans, *J. Geophys. Res.*, *112*, F02026, doi:10.1029/2006JF000610.

1. Introduction

[2] Alluvial fan formation has characteristically been described in terms of primary (depositional) and secondary (surficial reworking) fluvial processes [*Blair and McPherson*, 1994]. In arid environments, eolian processes can constitute a third process significant in fan evolution. Portions of alluvial fans and piedmonts located downwind from eolian sources are subjected to repeated transport of windblown sediment across their surfaces. The amount of windblown sediment deposited on piedmonts is a function of distance from sediment sources, prevailing wind directions, and the vegetation and relief of the substrate. While particles smaller than about 60 μm can enter suspension and be deposited far from the location of entrainment [*Pelletier and Cook*, 2005], larger sand-sized grains are transported primarily by saltation and are limited to transport within about 2 m of the surface [*Reheis*, 1999; *Greeley and Iversen*, 1985; *Marticorena and Bergametti*, 1995]. For this reason, sand-dominated eolian transport may be limited to pathways where surface roughness (i.e., pavement and vegetation) and relief are continuously low enough for entrainment to occur. The purpose of this study is to quantify the threshold conditions for transport of fine and coarse sand on alluvial fans using a numerical model and to test the model predictions at two playas in Clark County, Nevada.

[3] Late Cenozoic cutting-and-filling cycles have produced nested terraces on many fans that rise like a flight of stairs from the active channel. These stairs are characterized by a systematic decrease in along-strike fan-surface relief from the head to toe of the fan. The degree of channel entrenchment decreases with distance from the fan apex as the terrace treads of older fan surfaces and the active channel converge. Here we test our hypothesis that when located near a source of sandy material, portions of the fan surface exhibiting low relief allow eolian transport by saltation, resulting in a swath of deposition of sandy material across the distal fan surface. In contrast, we propose that zones of greater relief in the proximal fan region serve as traps for saltating material, thereby inhibiting eolian deposition across the fan surface. Because the gradient between fan terraces and active channels converges at a similar rate across the fans observed in this study, the threshold relief and resulting swath of eolian deposition by saltation approximately follows contour (Figures 1b–1e). Fine-grained sediment in channels transported by fluvial processes into zones of lower relief is also available for transport by saltation. This same sediment in the higher-relief zone of the fan is sheltered from winds that could

[1]Department of Geosciences, University of Arizona, Tucson, Arizona, USA.

0148-0227/07/2006JF000610

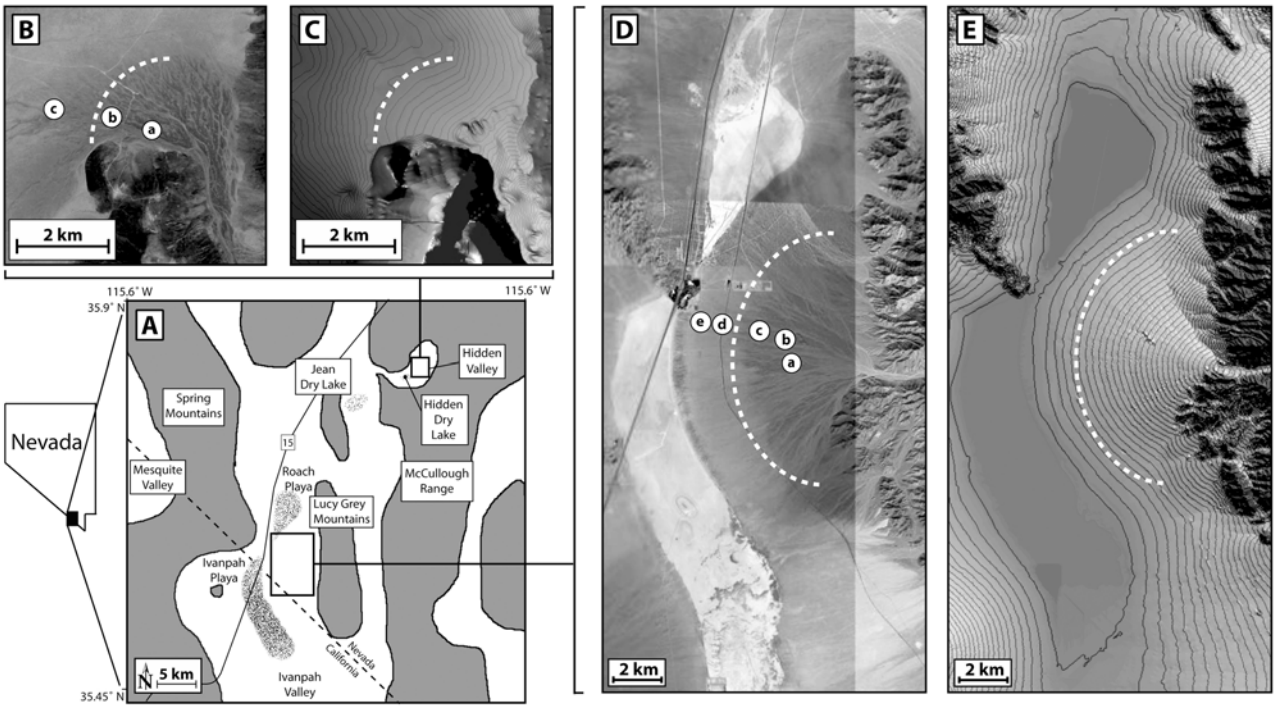

Figure 1. (a) Location map of Ivanpah and Hidden Valley field areas, Clark County, Nevada. (b–e) Quickbird and shaded relief image with topographic contour line overlay for the Hidden Valley and Lucy Grey Fans. Lettered circles correspond with measured topographic profile locations shown in Figures 4 and 5. The dashed line in each figure represents the upper boundary of the observed eolian corridor. Below this boundary, sand-dominated eolian transport occurs everywhere. Above this boundary, saltation is inhibited by higher fan relief and occurs only locally, perhaps only under extreme wind conditions.

otherwise exert sufficient shear stress to initiate saltation of material from channel to terrace.

[4] While research has been devoted to accurately measuring threshold sediment mobilization values in the field [*Marticorena et al.*, 1997a, 1997b; *Lancaster and Baas*, 1998] and using field-collected data [*Pelletier*, 2006], the majority of studies have taken place in wind tunnels under controlled conditions [*Raupach*, 1992; *Dong et al.*, 2002; *Hagen*, 1999; *Nishimura and Hunt*, 2000]. Our study combines the multispectral finite difference (MSFD) model with natural particle size and wind data to realistically model boundary layer surface flow over alluvial fan topography. Our approach blends laboratory-tested sediment transport equations with numerical modeling calibrated with field data to predict where saltation is able to operate most effectively under natural conditions.

2. Study Area and Field Observations

[5] Our study area is located in both Ivanpah and Hidden Valley along the western front of the Lucy Grey and McCullough Ranges in Clark County, Nevada near the California border (Figure 1a). Each valley contains an alluvial fan located in close proximity to one or more playas. In Ivanpah Valley, a large fan sourced from the Lucy Grey Mountains terminates adjacent to both Roach Lake and Ivanpah Playa (Figure 1a). Our second study site in Hidden Valley is located approximately 30 km to the northeast of Ivanpah Playa. Here a smaller fan sourced from the McCullough Range grades toward Hidden Dry Lake (Figure 1b). Both fans exhibit a swath of eolian deposition on their distal reaches where relief between terrace and active channel is lower relative to proximal portions of the fan. Here we use ''proximal'' and ''distal'' to describe location within the piedmont, not proximity to the source of eolian sediment (i.e., playas). A series of playas, sand ramps, and an overall drape of sandy, windblown material links multiple valleys in this portion of Nevada, forming a large-scale eolian ''corridor'' (K. House, personal communication).

[6] Abandoned terraces on both fans exhibit varying degrees of pavement maturity, rock varnish development, remnant microtopography, and planarity depending on age of deposition. The oldest terraces stand highest on the fan; younger terraces are inset into older alluvium, demonstrating the traditional sequence of quaternary fan terraces commonly observed in the southwestern United States [*Bull*, 1991]. The overall relief between abandoned terrace and active channel decreases from proximal to distal fan. The overall quality of desert pavement on all aged surfaces abruptly diminishes upon entering the ''corridor'' zone due to the high fluxes of windblown sand passing across lower relief portions of the fan. Terraces straddling this boundary exhibit well-varnished pavements with nearly complete interlocking clast coverage upfan from the boundary, and progressively more degraded, sparse clast coverage moving downfan, yielding to sandier deposition downfan from the boundary.

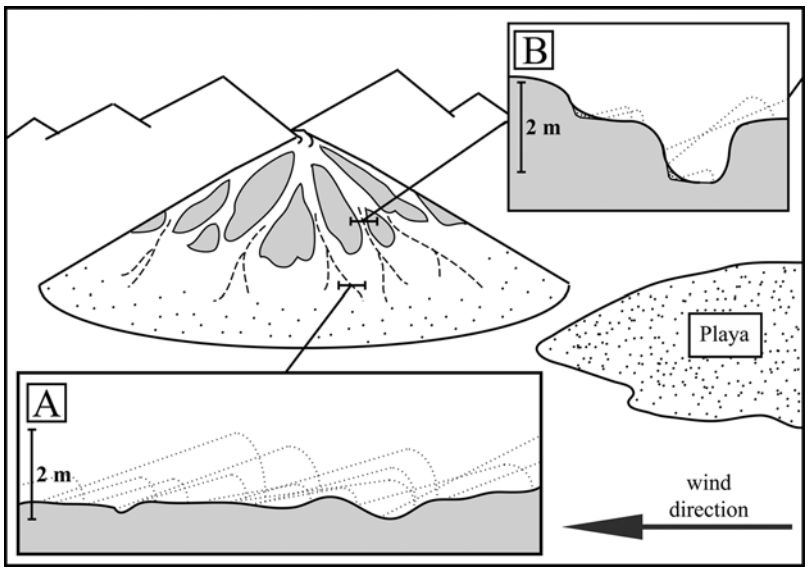

Figure 2. Schematic diagram of fan profiles. (a) Example of distal fan profile. Dashed lines represent grain saltation trajectories unimpeded by low fan relief. (b) Example of midproximal fan profile. Here saltating grains become trapped in high relief areas between channel and terrace. Traps accumulate windblown sand which can be remobilized under extreme wind conditions or transported downfan by fluvial processes.

[7] To accurately represent topography and relative relief from proximal to distal fan for input to MSFD modeling, profiles spanning multiple terrace ages were measured on each fan normal to the channel orientation. Profiles were measured using a tripod-mounted total station positioned on a highstanding terrace to ensure uninterrupted line-of-sight with the pole-mounted prism. Profile point spacing averaged approximately 2 m, although smaller transect steps were used where detailed topography was encountered. While overall relief between active channel and abandoned terrace increased from distal to proximal fan (Figure 2), some variation in this trend was observed. This is reflected in our transect data by portions of transects from the middle to upper fan exhibiting slightly higher relief than transects conducted higher on the fan. This reversal from the expected trend is minor and occurs only locally.

3. Model Description

3.1. Boundary Layer Model Component

[8] In order to compute the turbulent shear stresses over different fan profiles, we developed a numerical modeling code based on the mixed-spectral finite difference (MSFD) code developed and tested by *Walmsley et al.* [1982], *Beljaars et al.* [1987], *Xu and Taylor* [1995], *Karpik et al.* [1995], and *Taylor* [1998]. MSFD is a boundary layer model that solves the Reynolds-stress equations for boundary layer flow over arbitrary topography and surface roughness. The advantage of the model is its computational speed and ease of use. A limitation of the model, however, is that it does not calculate the detailed flow structure of recirculation zones behind topographic obstacles and it loses accuracy for rapidly varying topography and surface roughness. MSFD has been applied to other problems in eolian geomorphology by *Howard* [1978].

[9] MSFD works on a uniformly spaced grid in the horizontal direction and a logarithmically spaced, terrain-following grid in the vertical direction. The vertical coordinate is given by the local distance above the ground surface, $Z = z - f$, where f is the local ground-surface height. Grid points in the vertical direction range from values much lower than the roughness length, z_0, to values much greater than the topographic relief. For example, if z_0 is 0.01 m and the total relief of the profile is 2 m, a reasonable set of values for the vertical coordinate system is 0.001, 0.00333, 0.01, 0.0333, ... 33.3, and 100 m, for a total of 11 grid points in the vertical direction.

[10] The model solves the linearized Reynolds stress equations assuming mixing-length closure by working in the Fourier, or wave number, domain. The equations for the perturbed velocities and shear stresses in two dimensions (2D) are given by

$$ik u_0 \hat{u}_1 + \frac{du_0}{dZ}\hat{w}_1 = -\frac{1}{\rho} ik \hat{p}_1 + \frac{\partial \hat{\tau}_{x1}}{\partial Z} \tag{1}$$

$$ik u_0 \hat{w}_1 - k u_0 \hat{f}_1 = -\frac{1}{\rho}\frac{\partial \hat{p}_1}{\partial Z} \tag{2}$$

$$ik\hat{u}_1 + \frac{\partial \hat{w}_1}{\partial Z} = 0 \tag{3}$$

$$\hat{\tau}_{x1} = 2\kappa(Z + z_0)u_* \frac{\partial \hat{u}_1}{\partial Z} \tag{4}$$

$$u_0 = \frac{u_*}{\kappa} \ln\left(\frac{Z + z_0}{z_0}\right) \tag{5}$$

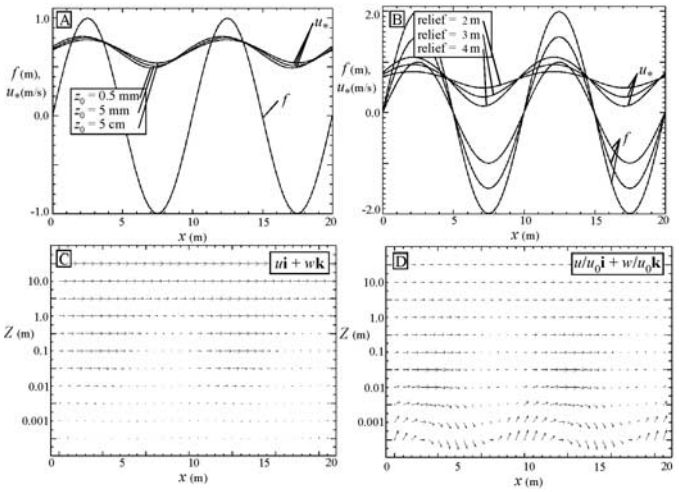

Figure 3. (a) Example of model output over idealized topography (sine wave) with variations in bed roughness. (b) Example of model output over varying topographic relief (sine wave with varying amplitude). Modeled shear velocity patterns are affected to a much greater extent by topographic relief than surface roughness. (c) Vector plot of actual wind velocities at logarithmically spaced heights above the bed as predicted by MSFD modeling. (d) Modeled wind velocities normalized by logarithmic profile to accentuate velocity perturbations near the bed.

where k is the wave number, u and w are the velocities in the horizontal (x) and vertical (z) directions, respectively, p is the pressure, τ_x is the shear stress, f is the topography, u_* is the unperturbed shear velocity, κ is the von Karman constant (0.4), the subscripts 0 and 1 represent the mean and perturbed values for each variable (the mean is the value if the topography was flat), and the hat above each variable indicates a Fourier transform. Each Fourier-transformed variable represents both real and imaginary parts (for example, $\hat{u}_1 = \hat{u}_{1r} + i\hat{u}_{1i}$, where $\hat{u}_{1r}$ and $\hat{u}_{1i}$ are the real and imaginary parts of $\hat{u}_1$). Equations (1)–(4) represent eight total equations because the real and imaginary part of each variable must be calculated. Equations (1)–(5) are identical to equations (6), (7), and (9) of *Beljaars et al.* [1987] assuming two-dimensional flow. The wind and stress fields for each wave number comprise a one-dimensional (1D) two-point boundary value problem for eight simultaneous ordinary differential equations (ODEs). This type of problem can be solved using a shooting method [*Press et al.*, 1992].

[11] MSFD works with periodic boundary conditions (i.e., the downwind end of the grid wraps around to the upwind end). Due to the Fourier-transformed nature of the model, MSFD works most simply when the number of horizontal grid points is a power of two. If this is the case, fast Fourier transform (FFT) techniques can be directly used to solve the equations with no additional processing. A no-slip boundary condition is enforced at the ground surface (i.e., the velocities and pressures go to zero). Far from the ground, the effects of variable topography and surface roughness variations go to zero. At the upper end of the grid, the perturbed values of all of the model variables go to zero. Mathematically, these boundary conditions are given by

$$\hat{u}_1 = \hat{w}_1 = \hat{p}_1 = 0 \quad \text{at} \quad Z = 0 \tag{6}$$

$$\hat{u}_1 = \hat{w}_1 = \hat{p}_1 = \hat{\tau}_1 = 0 \quad \text{at} \quad Z = \infty \tag{7}$$

In the model, the boundary conditions at $Z = 0$ are enforced at some very small distance from the ground (i.e., $Z = 0.001$ or smaller). Similarly, the upper boundary conditions are enforced at a large distance (for example, Z = 100 m for low-relief topography).

[12] The input data required to solve equations (1)–(5) are the topographic profile [Fourier-transformed for use as $\hat{f}_1$ in equation (2)], the surface roughness z_0 (assumed here to be uniform for each profile), and the unperturbed shear velocity u_*. Topographic profiles surveyed in the field were first preprocessed for input. The profiles were resampled by linear interpolation so that each profile had a number of values equal to a power of two. Second, the profile was made periodic by computing the mirror image of the profile and adding it to the end of the original profile. In this way, a profile with indices from 1 to 256 would become a profile of length 512 with indices 1... 256, 256... 1. These preprocessing steps enable the input data to be consistent with the periodic boundary conditions used by the model, and they have the effect of minimizing "edge effects."

[13] Examples of the model output are given in Figure 3 for idealized topography (i.e., a sine wave given by $f = A \sin(2\pi x/\lambda)$), illustrating the sensitivity of model results to variations in bed roughness (Figure 3a) and topographic relief (Figure 3b). In Figure 3a, the topography f is plotted together with the model-predicted values of u_* along each profile. Our "reference" case for these runs uses z_0 = 5 mm, λ = 10 m, A = 2 m, and u_* = 0.67 (corresponding to 10 m/s at a height 2 m above the ground). Figure 3a also includes the u_* profiles resulting from model runs with z_0 values ten times larger (5 cm) and smaller (0.5 mm) than the reference value. The shear velocities in Figures 3a and 3b follow the sinusoidal topography with the maximum shear velocity located slightly upwind from the crest. The shear velocity pattern depends only weakly on surface roughness, with slightly larger spatial variations and downwind shifts

resulting from rougher beds. The effects of variable relief are shown in Figure 3b. In these cases, the amplitude of the sine wave was varied between A = 1, 1.5, and 2 m while keeping all other parameter values the same as in the reference case. These results show that greater relief causes larger spatial variations in shear velocity. In other words, shear stresses are greater above crests and lower above troughs at the relief increases. This suggests that as relief increases, a critical point will eventually be passed where sand cannot be transported through the troughs because the shear velocity falls below the threshold value.

[14] Figures 3c and 3d illustrate vector plots of wind velocity predicted by MSFD for the reference case. Figure 3c illustrates the actual wind velocity at logarithmically spaced heights Z above the bed. Figure 3d illustrates the velocity normalized by the logarithmic profile, which allows for the velocity perturbations close to the bed to be more clearly illustrated (i.e., velocity perturbations increase toward the bed, but the velocity also goes to zero there, so Figure 3d is designed to magnify the bed effects). These figures illustrate the speed-up in velocity over crests associated with flow convergence and the slow-down over troughs caused by flow divergence. This effect extends a distance above the bed roughly equal to the bed relief.

3.2. Effects of Local Topography on Critical Shear Velocity

[15] Variations in topography actually influence eolian transport in two distinct ways. Figure 3b clearly illustrates how topographic variations cause shear-velocity variations. This is a purely aerodynamic effect. The local terrain plays an additional role, however, because movement of sand from a trough requires not only that sand particles be lifted, but that they be lifted with sufficient vertical force to move them uphill. This additional shear stress associated with variations in bed slope was studied by *Hardisty and Whitehouse* [1988]. In their study of sand transport in the Sahara, they endorsed a correction factor proposed by *Dyer* [1986] in which the threshold shear velocity is given by

$$u_{*_c} = u_{*_{c0}} \sqrt{\frac{\tan\phi + \frac{\partial f}{\partial x}}{\tan\phi \sqrt{\left(\frac{\partial f}{\partial x}\right)^2 + 1}}} \tag{8}$$

where u_{*c0} is the critical shear velocity for flat terrain and ϕ is the angle of internal friction. The correction factor equals 1 for flat topography, goes below 1 as the downwind bed slope increases (i.e., as $\partial f/\partial x$ becomes more negative), and eventually becomes zero at the angle of internal friction. This behavior is consistent with the fact that very little shear stress is required to transport sand close to the angle of repose. If the downwind bed slope is positive (i.e., sand must move uphill), the threshold shear velocity increases, but more slowly than for the downhill side of the curve.

3.3. Model Calibration

[16] Because no wind gauge data was available for the study areas, wind velocity data for three similarly vegetated piedmonts, twin springs, immigration wash, and oriental wash (CEMP and RAWS stations, http://www.wrcc.dri.edu/wraws/nvutF.html) in Nevada were obtained and processed according to the von Karman-Prandtl "law of the wall":

$$u_* = \frac{u_z k}{\ln\left(\frac{z}{z_0}\right)} \tag{9}$$

where u_* is shear velocity, u_z is wind velocity measured at height z, k is the Von Karman constant, and z_0 is the roughness length. Although the dominant wind direction for our field areas cannot be inferred from these wind stations, wind directions in the Basin and Range province are generally parallel to the valley aspect (in this case roughly n-s) and reverse seasonally. This direction corresponds to the observed transport and deposition patterns observed in our field areas. Vegetation on both fans is predominantly composed of creosote, saltbush, and Mojave Yucca. To approximate z_0 values we utilized the roughness density approach outlined by *Marticorena et al.* [1997a, 1997b] and *Raupach et al.* [1993]:

$$\lambda = \frac{nbh}{S} \tag{10}$$

where λ is the roughness density, n is the number of roughness elements, b is the mean breadth, h is the mean height, and S is the area being considered. For roughness densities greater than 0.11, z_0 is set equal to $(0.05)h$ [*Marticorena et al.*, 1997a, 1997b; *Raupach et al.*, 1993; *Okin et al.*, 2006]. Average vegetation size and density easily exceeded roughness densities of 0.11 in both field areas. With an average vegetation height of approximately 1 m, a z_0 value of 0.05 m was used for model runs.

[17] Two years of daily average wind velocity data (12 months prior to and following the date of station photos) for three stations was analyzed, and u_* values for winds exceeding the 90th percentile intensities were calculated. This range was chosen in an attempt to identify an "extreme" shear velocity capable of mobilizing significant amounts of sediment, yet occurring with enough frequency to be geomorphically effective [*Wolman and Miller*, 1960]. Percentile wind velocity values for all three wind stations were in close agreement, yielding extreme u_* values ranging from approximately 0.38–0.72 m/s (corresponding with the lowest 90th and highest 99.9th percentile u_* value, respectively). In this paper we choose a u_* value at the low end of this range (0.40 m/s) in order to illustrate the model behavior. Unfortunately, we cannot further constrain the u_* value at our study sites because it is difficult to uniquely choose an "extreme" velocity. Our study sites will experience shear velocities across the full range from 0.38 to 0.72 m/s, but the larger wind speeds may not occur with sufficient frequency to contribute significantly to the overall sand flux.

[18] To accurately determine critical shear velocity for our field areas, channel sediments, proximal and distal fan terrace eolian epipedons, and playa surfaces were sampled and analyzed for particle size distribution. Because many of the samples contained pieces from the eolian epipedon, aggregates were broken up prior to sieving using a mortar and pestle. Samples were separated into 6 size fractions

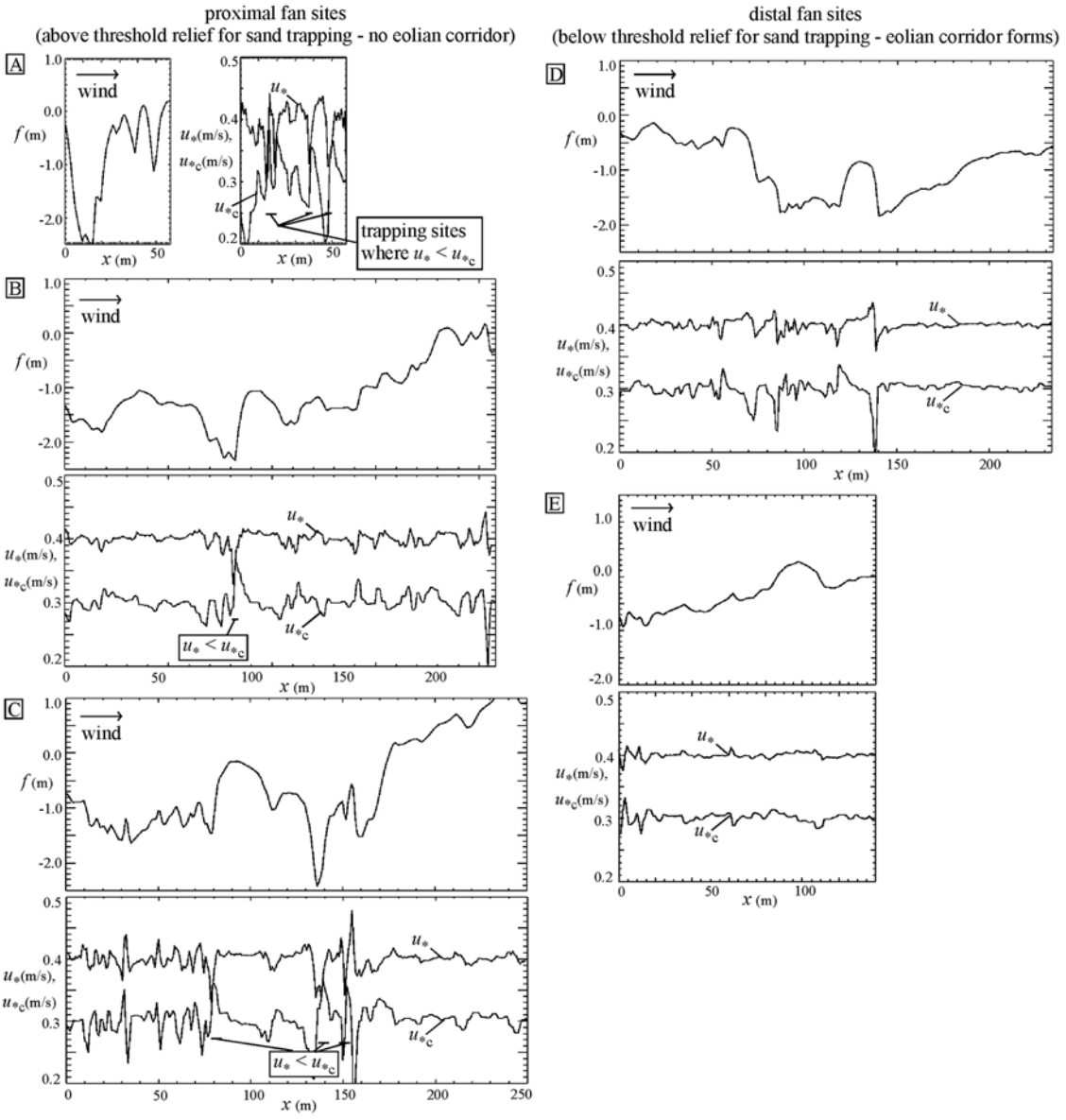

Figure 4. MSFD model results for Lucy Grey field area. In each plot, the upper diagram is the measured topographic profile while the lower plot depicts model results from (a) proximal to (e) distal fan. The top line in each lower plot represents the predicted u_* values along the profile. The bottom line is the predicted u_{*c} value required for sediment transport along the same profile. Where these lines intersect, modeled shear velocities are less than those required to transport sediment, and trapping occurs. Multiple traps exist in (a–c) the proximal fan, potential traps exist where predicted u_* and u_{*c} values nearly intersect in the transitional profile near (d) the eolian corridor boundary, and no trapping occurs in (e) the distal fan where sand transport can occur everywhere.

ranging from very coarse sand (2000–1000 μm) to very fine sand (125–63 μm) and sediment passing through all screens (<63 μm) using a sieve-shaking machine. A grain diameter range of 250–500 μm (medium sand) was chosen for model input based on the absence of medium sand in proximal piedmont deposits compared to channel sediments (Figure 6b). The presence of finer sediments in proximal piedmont as well as channel sediments indicates these sized particles are transported across the entire fan regardless of relief. Larger grains are surely moved, but on a more infrequent timescale. For model input, u_{*c} was calculated using *Bagnold*'s [1941] critical shear velocity calculation:

$$u_{*_c} = A\sqrt{\frac{\rho_s - \rho_a}{\rho_a} gD} \tag{11}$$

where A is a constant of proportionality (equal to 0.1 for air), ρ_s is the density of sediment, ρ_a is the density of air, g is the acceleration due to gravity, and D is grain size diameter.

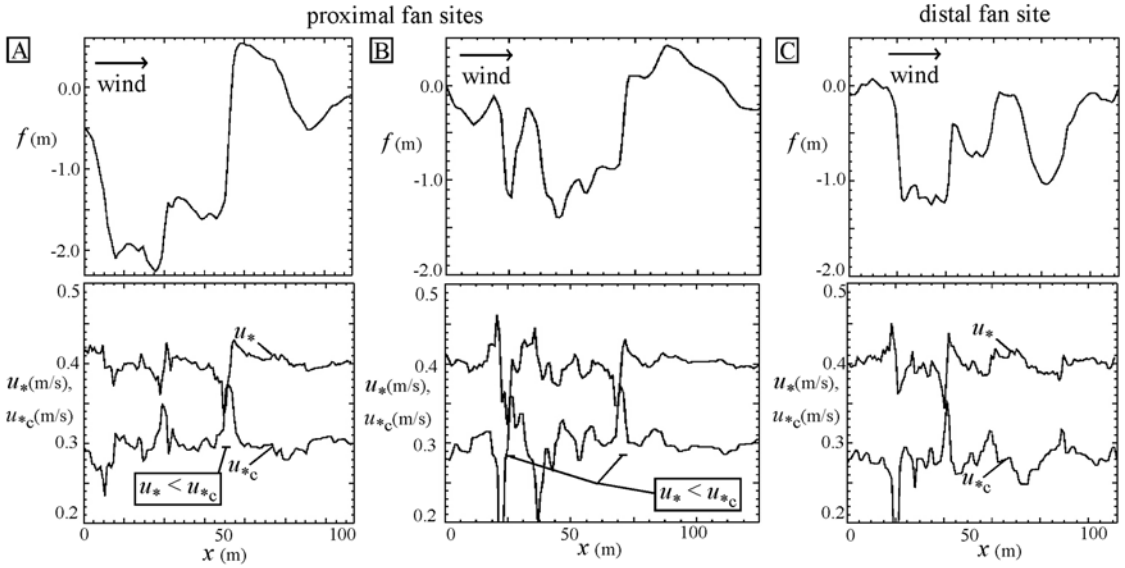

Figure 5. MSFD model results for the Hidden Valley Fan field area. Plots follow the same arrangement as those in Figure 4. Multiple sediment traps exist in (a and b) the upper fan profiles where relief is highest. (c) Although some trapping is still predicted in the lowest profile, overall relief is less than relief measured in Figures 5a and 5b. The rate of change in relief is also important for sediment trapping ability. An abrupt topographic rise inhibits saltation more effectively than a gradual topographic rise of the same relief. For example, a vertical cut bank >1 m effectively stops windblown sediment whereas a gradual slope of similar relief allows saltation to operate.

For medium quartz sand, the critical shear velocity ranges from approximately 0.22 m/s for $D = 250$ μm to 0.32 m/s for $D = 500$ μm. It is important to note that our use of "critical shear velocity" refers to the shear stress required to initiate saltation, not maintain it (i.e., static, not dynamic shear velocity). Because static shear velocity is greater than dynamic shear velocity, modeled zones of sediment transport may continue to allow saltation at u_* values less than u_{*c} once static shear velocities have been exceeded. Equation (11) has been tested in numerous wind tunnel studies under controlled conditions, including uniform D. Because our study involves heterogeneous natural sediments, the calculated value for u_{*c} may underestimate the true threshold value for our study sites.

3.4. Model Results for the Study Areas

[19] MSFD model runs using field calibrated parameters and measured fan profiles recreate the eolian "corridor" effect at approximately the same fan elevation observed in the study areas. Modeled u_* and u_{*c} values along fan profiles are represented by the uppermost two plots in Figures 4 and 5. Where the upper plot, representing u_*, intersects the lower plot, representing u_{*c}, modeled shear velocity is less than the critical shear velocity required for sediment transport as determined by roughness elements, local slope, and topography. Physically, sand already in transport at these locations along the profile would drop out of transport due to decreased shear velocities owing to flow divergence and locally higher u_{*c} values due to downwind bed slope. In essence, these areas constitute sediment "traps". Sediment deposited in these traps due to insufficient shear velocity is difficult to remobilize as it is sheltered from winds by locally higher relief and is likely only susceptible to subsequent eolian transport under extreme wind conditions. High relief profiles provided multiple trapping zones for windblown sediment (Figure 4a) whereas low relief profiles lack traps and allow transport by saltation everywhere, i.e., $u_* > u_{*c}$ along the entire profile (Figure 4e).

[20] The observed onset of eolian deposition on the Lucy Grey Fan occurred very close to our fourth profile downfan (Figure 4d). The model predicts eolian transport across this portion of the fan, with a few locations along the profile which approach trapping topography levels. Pavements in this area of the fan were observed to be degraded compared to similar-age pavements farther up the fan. The locally higher influx of sandy material likely inundates pavement in lower relief portions of the fan, accumulating more rapidly than sediment can be added to the Av horizon beneath pavement clasts. Downfan from the location of this transitional profile, both fine and coarse sand can be transported everywhere along the profile as u_* is uniformly greater than u_{*c}. Although not as clear as the Lucy Grey Fan profiles, model results for the Hidden Valley Fan are similar. Overall relief on the proximal fan profile exceeds 2 m and provides multiple sediment traps (Figure 5a). Lower fan profiles still exhibit a trapping capability, but to a lesser extent in the distal fan.

[21] Contrary to our expected result, percent medium and coarse sand is greater in several transects in the proximal fan compared to those in the distal fan. Grain size distributions from channel sediments exhibit abundant medium to very coarse sand, which designates them as likely sources for the coarse material found in proximal fan deposits (Figure 6b). The abundance of coarse sediment found in fan channels compared to the relative paucity of coarse material observed

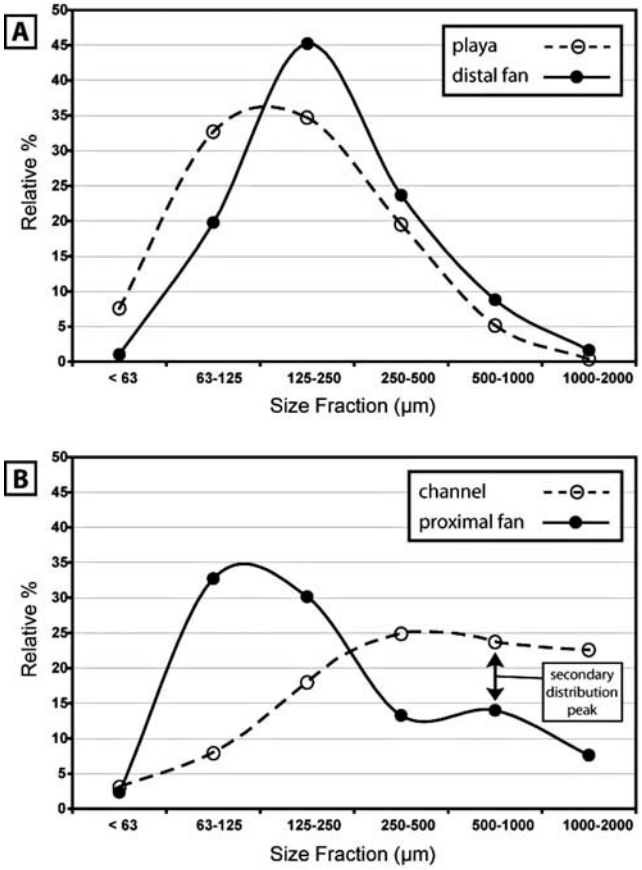

Figure 6. Grain size distributions for sediment samples collected along field transects. (a) Particle size distributions for distal Lucy Grey Fan deposits and Ivanpah Playa. The unimodal grain size distribution is very similar in both samples, particularly for grains larger than 125 μm. This similarity indicates the playa is the dominant source of windblown sediment in the distal fan. (b) Particle size distributions for proximal Lucy Grey Fan deposits and channel sediments. Proximal deposits exhibited a bimodal distribution with a secondary peak in the coarse sand fraction. This particle size is abundant in nearby channel sediments indicating that proximal deposits are partially sourced from coarser channel sediments.

in proximal piedmont eolian epipedons indicates medium sand (250–500 μm) is the critical grain size for which relief is a factor for eolian transportability in our field areas. Grain size analysis for distal fan transects and Ivanpah Playa is strikingly similar (Figure 6a), indicating that the playa is the dominant source of eolian material for the lower fan and that all available sediment is readily transported across the surface due to low relief. The presence of coarse sediment in eolian epipedons of proximal fan terraces indicates some transport of channel material must occur even though many sediment traps exist in this portion of the fan. It is possible that this transport occurs under extreme wind conditions capable of mobilizing larger sand grains from zones of high relief. In this sense, the upper fan "sees" the channels as a source of sediment under extreme wind conditions while the lower fan "sees" both channel and playa sediments as sources, although the playa is clearly the dominant source. It is also possible that the larger grains observed in proximal piedmont surfaces were deposited by sheetwash or other fan-building processes before relief between terrace and channel was significant. Very fine-grained sediment in suspension sourced from local playas as well as other regional sources is likely deposited over the entire fan as its transport mechanism is not hindered by fan relief.

4. Discussion

[22] Model output is based on u_* and D values chosen from a range of possible field-calibrated values. While our best estimate of these parameters results in model output which closely matches the observed location of the onset of eolian transport across the fan, it is also possible that other combinations of these parameters will result in reasonable model output as well. For example, choosing a lower u_{*c} value would result in modeled eolian transport initiating in higher relief portions of the fan. This effect could be counterbalanced by using a lower estimation of u_*, resulting in model output similar to our initial results.

[23] The precise location of the observed eolian threshold cannot be definitively predicted by MSFD modeling. This is due primarily to uncertainty in the unperturbed shear velocity representing "extreme" wind conditions. In this paper we chose a value of 0.40 m/s, corresponding closely to the 90% percentile wind speed. There will, of course, be larger shear velocities exerted on the substrate (representing 99 and 99.9% percentiles, for example), but their relative rarity of these extreme wind speeds may prevent them from developing an eolian corridor. Despite this uncertainty, the model does show that a threshold condition exists for eolian transport, how the threshold condition is controlled by relief, grain size, and surface roughness, and that the threshold position is approximately where we observe it in the field using reasonable input parameter variables. Better constraint of threshold shear velocities and establishment of geomorphically most effective wind speeds are both candidates for future work pertaining to MSFD modeling of boundary layer flow and the influence of topography on eolian transport.

[24] Although model output was shown to be relatively insensitive to z_0, the value for z_0 has significant influence on calculated u_* values which, in turn, have influence on model output. Unfortunately, the characterization of z_0 with respect to vegetation is a difficult task. The roughness density approach used here quantifies the mean frontal area of vegetation elements which absorb a portion of the shear stress otherwise available to act on the surface and transport sediment [*Raupach et al.*, 1993]. Possible modifications to the roughness density approach include consideration of vegetation flexibility and patterns in unvegetated areas, or "plant-interspaces" [*Okin et al.*, 2006]. In wind tunnel studies under ideal conditions z_0 is equal to 1/30 the grain size diameter. In our natural study areas, z_0 is a combination of roughness elements on various scales. Small-scale roughness elements such as pavement clasts, microtopography, and vegetation are superimposed on fan topography. The need for better approximation of z_0 values in the field has been previously expressed by *Blumberg and Greeley* [1993] and *Lancaster et al.* [1991].

[25] The location and extent of eolian corridors is important for hydrologic and pedologic studies. Windblown dust and sand compose a large percentage of pedologic material in late Pleistocene and Holocene soils in arid environments [*Reheis et al.*, 1995]. The amount of sand present in soil epipedons influences rates of infiltration and leaching which, in turn, affect depth to carbonate and other illuvial subsurface horizons. Pulses of eolian sediment can affect rates of soil genesis so significantly that steady state, linear models for soil horizonation and genesis have been shown to be inapplicable for soils forming downwind of significant sources of windblown sediment (i.e., playas or eolian corridors) [*Chadwick and Davis*, 1990].

5. Conclusions

[26] The existence of a relief threshold for sand transport by saltation is evident based on field and aerial photo observations as well as modeling. Zones of low relief permit transport of all available grain sizes while zones of higher relief provide more sediment traps and offer more resistance to sediment transport, particularly medium to coarse sand. Better constraint of model parameters combined with a more sophisticated approach for simulating complex roughness elements such as vegetation is important for future studies. Combining MSFD modeling of eolian transport by saltation with existing advection diffusion models of dust plume deposition [*Pelletier and Cook*, 2005] can provide a comprehensive view of eolian activity at subbasin to basin scales.

[27] **Acknowledgments.** Kyle House for helpful conversations regarding eolian corridors and the surficial geology of Ivanpah Valley. We gratefully acknowledge the support by the Army Research Office Terrestrial Sciences Program, grant W911NF-04-1-0266.

References

Bagnold, R. A. (1941), *The physics of blown sand and desert dunes*, CRC Press, Boca Raton, Fla.

Beljaars, A. C. M., J. L. Walmsley, and P. A. Taylor (1987), A mixed spectral finite difference model for neutrally stratified boundary layer flow over roughness changes and topography, *Boundary Layer Meteorol.*, *38*, 273–303.

Blair, T. C., and J. G. McPherson (1994), Alluvial fans and their natural distinction from rivers based on morphology, hydraulic processes, sedimentary processes, and facies assemblages, *J. Sediment. Res. Sect. A Sediment. Pet. Process.*, *64*, 450–489.

Blumberg, D. G., and R. Greeley (1993), Field studies of aerodynamic roughness length, *J. Arid Environ.*, *25*, 39–48.

Bull, W. B. (1991), *Geomorphic responses to climatic change*, Oxford Univ. Press, New York.

Chadwick, O. A., and J. O. Davis (1990), Soil-forming intervals caused by eolian sediment pulses in the Lahontan Basin, northwestern Nevada, *Geology (Boulder)*, *18*, 243–246.

Dong, Z. B., X. P. Liu, and X. M. Wang (2002), Aerodynamic roughness of gravel surfaces, *Geomorphology*, *43*, 17–31.

Dyer, K. R. (1986), *Coastal and estuarine sediment dynamics*, John Wiley, Hoboken, N. J.

Greeley, R., and J. D. Iversen (1985), *Wind as a geological process on Earth, Mars, Venus, and Titan*, Cambridge Univ. Press, New York.

Hagen, L. J. (1999), Assessment of wind erosion parameters using wind tunnels, paper presented at Sustaining the Global Farm, International Soil Conservation Organization, Purdue University, West Layfayette, In., 24–29 May.

Hardisty, J., and R. J. S. Whitehouse (1988), Evidence for a new sand transport process from experiments on Saharan dunes, *Science*, *332*, 532–535.

Howard, A. D. (1978), Sand transport model of barchan dune equilibrium, *Sedimentology*, *25*, 307–338.

Karpik, S. R., J. L. Walmsley, and W. Weng (1995), The mixed spectral finite difference (MSFD) model: Improved upper boundary conditions, *Boundary Layer Meteorol.*, *75*, 353–380.

Lancaster, N., and A. Baas (1998), Influence of vegetation cover on sand transport by wind: Field studies at Owens Lake, California, *Earth Surf. Process. Landf.*, *23*, 69–82.

Lancaster, N., R. Greeley, and K. R. Rasmussen (1991), Interaction between unvegetated desert surfaces and the atospheric boundary layer: A preliminary assessment, *Acta Mech. Suppl.*, *2*, 89–102.

Marticorena, B., and G. Bergametti (1995), Modeling the atmospheric dust cycle: 1. Design of a soil-derived dust emission scheme, *J. Geophys. Res. Atmos.*, *100*, 16,415–16,430.

Marticorena, B., G. Bergametti, B. Aumont, Y. Callot, C. Ndoume, and M. Legrand (1997a), Modeling the atmospheric dust cycle: 2. Simulation of Saharan dust sources, *J. Geophys. Res. Atmos.*, *102*, 4387–4404.

Marticorena, B., G. Bergametti, D. Gillette, and J. Belnap (1997b), Factors controlling threshold friction velocity in semiarid and arid areas of the United States, *J. Geophys. Res. Atmos.*, *102*, 23,277–23,287.

Nishimura, K., and J. C. R. Hunt (2000), Saltation and incipient suspension above a flat particle bed below a turbulent boundary layer, *J. Fluid Mech.*, *417*, 77–102.

Okin, G. S., D. A. Gillette, and J. E. Herrick (2006), Multi-scale controls on and consequences of aeolian processes in landscape change in arid and semi-arid environments, *J. Arid. Environ.*, *65*, 253–275.

Pelletier, J. D. (2006), Sensitivity of playa windblown-dust emissions to climatic and anthropogenic change, *J. Arid Environ.*, *66*, 62–75.

Pelletier, J. D., and J. P. Cook (2005), Deposition of playa windblown dust over geologic time scales, *Geology*, *33*, 909–912.

Press, W. H., S. A. Teukolsky, W. T. Vetterling, and B. P. Flannery (1992), *Numerical Recipes in C: The Art of Scientific Computing Second Edition*, Cambridge Univ. Press, New York.

Raupach, M. R. (1992), Drag and drag partition on rough surfaces, *Boundary Layer Meteorol.*, *60*, 375–395.

Raupach, M. R., D. A. Gillette, and J. F. Leys (1993), The effect of roughness elements on wind erosion threshold, *J. Geophys. Res. Atmos.*, *98*, 3023–3029.

Reheis, M. C. (1999), Dust deposition and its effect on soils: A progress report, in *Desert winds: Monitoring wind-related surface processes in Arizona, New Mexico, and California.*, edited by S. Breed Carol and C. Reheis Marith, pp. 121–131, U. S. Geological Survey, Reston, VA, United States.

Reheis, M. C., J. C. Goodmacher, J. W. Harden, and L. McFadden (1995), Quaternary soils and dust deposition in southern Nevada and California, *Geol. Soc. Am. Bull.*, *107*, 1003–1022.

Taylor, P. A. (1998), Turbulent boundary layer flow over low and moderate slope hills, *J. Wind Eng. Ind. Aerodyn.*, *74*, 25–47.

Walmsley, J. L., J. R. Salmon, and P. A. Taylor (1982), On the application of a model boundary layer flow over low hills to real terrain, *Boundary Layer Meteorol.*, *23*, 17–46.

Wolman, M. G., and J. P. Miller (1960), Magnitude and frequency of forces in geomorphic processes, *J. Geol.*, *68*, 54–74.

Xu, D., and P. A. Taylor (1995), Boundary layer parameterization of drag over small-scale topography, *Q. J. R. Meteorol Soc.*, *121*, 433–443.

J. P. Cook and J. D. Pelletier, Department of Geosciences, University of Arizona, Gould-Simpson Building, 1040 East Fourth Street, Tucson, AZ 85721-0077, USA. (joe.cook@azgs.az.gov)